Cold Regions Science and Technology 174 (2020) 103063

Contents lists available at ScienceDirect

Cold Regions Science and Technology

journal homepage: www.elsevier.com/locate/coldregions

Analysis of acoustic emission characteristics of ice under three point bending

P. Datt[a,*], C. Chandel[a], V. Kumar[a], R. Sheoran[a,b], D. Nasker[a], J.C. Kapil[a], P.K. Srivastava[a]

[a] Snow and Avalanche Study Establishment (SASE), Chandigarh, 160036, India
[b] Panjab University (PU), Chandigarh, 160014, India

ARTICLE INFO

Keywords:
Acoustic emission (AE)
Ice deformation
Three point bending
AE amplitude
b-value
AE energy
RA parameter
Fracture mode identification

ABSTRACT

Acoustic emission (AE) is one of the promising techniques to understand the damage mechanism within a material and structural health monitoring non-invasively. The transient elastic energy released during the microscopic failure within a material is termed as acoustic emission. AE signals carry information about the mechanism and intensity of damage within a material. In this study, AE signatures were recorded during the mechanical loading of notched ice beams subjected to three point bending tests at three different strain rates i.e. $1 \times 10^{-5}\,s^{-1}$, $1 \times 10^{-4}\,s^{-1}$ and $1 \times 10^{-3}\,s^{-1}$. Various AE characteristics such as hits, amplitude, counts, rise time, energy release rate etc. were analysed in relation to the loading behaviour of ice beams. The AE amplitude distribution data was analysed to estimate b-value and its temporal variation throughout loading for all the three strain rate experiments. A decreasing trend in b-value with increasing bending stress was observed in all the three tests. Characterization of dominant failure mode was also attempted through the analysis of RA parameter and average frequency (AF) which indicates tensile mode as the dominant mode of fracture during three-point bending.

1. Introduction

Acoustic emission is a widely used non-destructive technique for assessment of progressive damage in various materials such as rocks, concrete, wood, composites etc. at both laboratory and larger scales (Lockner, 1993; Ohtsu, 1996; Vidya Sagar and Raghu Prasad, 2012; Bucur, 2006; Guarino et al., 1998; Amitrano et al., 2005). The stress waves within a material are the results of various non-reversible processes such as plastic deformation, crack opening, coalescence and growth of micro-cracks etc. Acoustic signal generated during the failure process propagates through the bulk and is detected at the surface by use of piezo transducers. The number of AE signals acquired by the detection system is related to the failure density or crack events occurred in the material. The nature of AE signal depends on the source and type of failure mode (Carpinteri et al., 2013). Various characteristics of AE waveform such as amplitude, rise time, energy and frequency carry information about the damage mode and fracture process (Carpinteri et al., 2013). Vidya Sagar and Raghu Prasad, 2012, recorded the energy released during fracture process in concrete and suggested that AE could be an efficient tool for fracture energy monitoring provided the attenuation of AE wave is not appreciable within the material. In fact, in most of the cases the AE wave undergoes attenuation during its propagation in material. Therefore, the measured AE energy can be in proportion and a small fraction of the released fracture energy during failure process. AE amplitude is one of the important parameter since it is related to the magnitude of failure event. However, the analysis of individual AE amplitude values can sometimes be misleading because the signal undergoes attenuation while propagating in the medium. Even a very high amplitude AE signal emitted at far could be recorded by the sensor as low amplitude (Shiotani et al., 2007). Therefore, relative distribution of AE amplitude is generally used to correlate the deformation process undergoing within the material. The b-value proposed by Gutenberg and Richter (1944) gives the relationship between frequency and magnitude of AE events emanated from a deformational process in a material. Investigations carried out by previous researchers suggest that there is a decrease in the b-value with increasing damage/micro-fractures within the material subjected to loading (Main et al., 1989; Lockner, 1993; Reiweger et al., 2015). Classification of cracking mode is another important area which is derived from the analysis of AE parameters i.e. RA parameter and average frequency (AF) (Ohno and Ohtsu, 2010; Shahidan et al., 2013; Li and Du, 2016). It was found that high RA and low AF values correspond to the shear crack whereas low RA and high AF correspond to the tensile crack. Researchers suggested that analysis of RA and AF along with the b-value can be used as a possible indicator of accelerating damage within a material which can lead to catastrophic failure.

* Corresponding author.
E-mail address: prem.datt@sase.drdo.in (P. Datt).

https://doi.org/10.1016/j.coldregions.2020.103063
Received 3 September 2019; Received in revised form 12 March 2020; Accepted 2 April 2020
Available online 03 April 2020
0165-232X/

Ice is one of the naturally occurring materials in the earth's cryosphere. Physical and mechanical properties of ice greatly affect the formation and dynamics of glaciers. Also, it is a cost effective construction material in cold regions for various applications such as embankment, highway and runways etc. (Masterson, 2009; Li and Du, 2016). Apart from the construction activities, ice in glaciated terrain poses a severe threat to the persons venturing in those areas. It provides a low friction sliding base to the newly fallen snow which is helpful in the formation of avalanches. Moreover, the Himalaya, having the highest glaciated peaks of the world witnesses hazards due to frequent ice cliff breaks (ice avalanches), crevasse openings etc. every year (Singh et al., 2013). In one such event 10 Indian soldiers got buried under deep snow and ice in Siachen glacier avalanche in Karakoram range of Indian Himalaya (Wikipedia, 2016). Prediction of such failure requires understanding of the damage mechanism of ice under different loading and temperature conditions. The plastic deformation of ice also contributes in the movement and break-up of glaciers over time (Andrews, 1985). Ice matrix is also the main component of snow structure and its mechanical properties determine the mechanical behaviour of snow (Chandel et al., 2014; Pinzer, 2009). The mechanical properties such as yield stress, fracture energy of ice are needed to implement the damage initiation and evolution law for micro-mechanical modelling of snow deformation (Chandel et al., 2014). In the past, various researchers have used acoustic emission to investigate the deformation of ice (Gold, 1960; Zaretsky et al., 1976; St Lawerence and Cole, 1982; Sinha, 1985, 1996; Sinha et al., 2012). Most of them have used the ring down count as the main AE parameter which is equivalent to the AE 'counts' in current AE systems. Other parameters such as amplitude, acoustic energy, b-value etc. were not correlated with the deformation process of ice. Recently, Li and Du (2016) attempted to correlate the acoustic emission signature to the ice deformation during compressive and three point beam loading tests in a laboratory setup. Authors analysed the AE parameters such as amplitude, rise time, counts, wave duration and energy in relation to the loading of samples. AE amplitude distribution data was further analysed for the calculation of b-value and its variation during the course of loading. They further suggested that analysis of AE features can be used to assess the onset of damage within the material. However, the analysis presented by them was based on only one displacement rate which was 2 mm/min which corresponds to strain rate: $1.6 \times 10^{-4}\ s^{-1}$.

From the above discussions, we can say that previously not much research was undertaken to study acoustic emission characteristics from ice. Therefore there is a need to investigate the deformation behaviour of ice to improve its understanding in terms of various AE parameters. In this work, we have taken the studies further by subjecting ice samples to bending load at three different strain rates and corresponding acoustic signature were detected and analysed to correlate the damage behaviour of ice. An analysis of dissipated energy components is carried out and comparison was made with the recorded acoustic energy. The variation of b-value, RA and AF was also analysed in relation to the evolution of damage.

2. Methodology

2.1. Sample preparation

An aluminium mould was used to make rectangular ice specimens in cold laboratory by freezing clean water at −9 °C. The irregularity and dimensions of the sample at outer boundaries were smoothened with the help of hot cutting wire. The ice samples were kept and tested inside cold laboratory at chamber temperature − 9 °C. A notch of approximately 12 mm was introduced with the help of a cutting blade in each sample. The size, shape and other details of the ice samples are given in Table 1.

2.2. Three point beam loading

The three point beam loading tests were conducted at cold laboratory, Snow and Avalanche Study Establishment (SASE), Manali, India. The experimental setup used in this study is shown in Fig. 1. It consists of a universal testing machine (UTM) with load cell of 5 kN, a console to control the machine and data acquisition system. The vertically moving plunger was modified with additional fixtures for loading the samples in three point beam configuration. The ice specimens were loaded at mid span with support at two ends during the test. The tests were conducted under displacement controlled mode and strain rate was derived from the displacement rate using Euler-Bernoulli beam theory (Appendix A). Depending on the specimen geometry, the displacement rate was determined to achieve the desired strain rate. Therefore, the displacement rates were 0.15 mm/min, 1.25 mm/min and 14.2 mm/min corresponding to strain rates $1 \times 10^{-5}\ s^{-1}$, $1 \times 10^{-4}\ s^{-1}$ and $1 \times 10^{-3}\ s^{-1}$, respectively.

2.3. Acoustic emission (AE) measurements

Multi-channel AE system from Physical Acoustics, USA was used for recording AEs generated from crack formation, extension and ultimate failure in the ice specimen. A more detailed description of AE system and related parameters is given elsewhere (Kapil et al., 2014; Datt et al., 2015). In the present experimental setup the AE sensors comprising of 03 resonant and 01 wideband were used. The sensors were directly coupled to the surface of ice specimen with the help of thin silicon grease layer. In fact mounting of sensors is crucial to reduce the acoustic impedance mismatch between the object under test and the AE sensor. Application of couplant provides better impedance matching which is further helpful to reduce the transmission losses of acoustic wave energy at sensor-specimen interface. Table 2 describes the details about the sensors used during the experimental measurements. The sensors were placed on both side of the loading line (Fig. 1). The noise level inside cold laboratory was measured with AE monitoring system and an amplitude threshold was selected as per the procedure discussed in Datt et al. (2015). After characterization of noise in the environmental chamber, the threshold amplitude was selected at 28 dB in order to remove the possible electronic and environmental noise. The experimental arrangement with AE sensors mounted on an ice specimen is shown in Fig. 1. One of the AE sensor i.e. R.45I developed some problem during the test, therefore its data was not analysed.

2.4. Data analysis

AE parameters recorded during the bending tests were analysed in relation to the load curve. An acoustic event is resulted due to the microscopic failure or any irreversible deformation undergoing in the bulk of material. However, detection of an event in the form of a transient electrical signal by a sensor is referred as 'Hit' (Hellier, 2003). An 'AE Hit' is recorded once the electrical signal generated by the sensor crosses the pre-decided threshold value. Various features such as amplitude, counts, rise time, wave duration, absolute acoustic energy etc. can be extracted from the waveform of AE signal (SAMOS AE system, User's Manual, 2005). In this study we have analysed AE features such as hit rate, amplitude, rise time, counts, wave duration and absolute AE energy in relation to the load curve/damage evolution within the ice specimen. AE Amplitude distribution data is used to calculate the temporal evolution of b-value, which is a measure of relative number of AE events with larger to smaller magnitudes. The b-value was defined by Gutenberg and Richter (1944) to establish a relationship between the magnitude of seismic activities and cumulative number of seismic events as expressed by Eq. 1.

$$\log_{10} N(M \geq M^{\circ}) = a - bM \quad (1)$$

where 'N' is the cumulative numbers of seismic events with magnitudes

Table 1
Geometrical parameters and strain rate of ice beams subjected to three point bending tests.

S. No.	Specimen length (L, mm)	Specimen breadth (b, mm)	Specimen height (d, mm)	Notch depth (a, mm)	Displacement rate (mm/min)	Strain rate (s^{-1})	Test index/ name
1	250	100	42	12	0.15	1×10^{-5}	3PBT_3Test
2	250	102	50	12	1.25	1×10^{-4}	3PBT_5Test
3	250	102	44	12	14.2	1×10^{-3}	3PBT_7Test

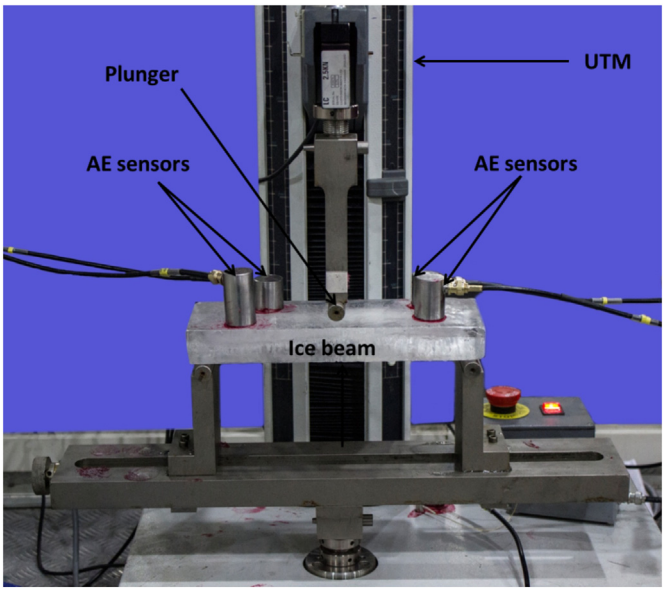

Fig. 1. Experimental set up consisting of universal testing machine (UTM) and AE sensors for thee point beam testing.

Table 2
Description of acoustic emission (AE) sensors used in the present investigation.

S.No.	Sensor model no	Frequency range (Resonant Frequency) (kHz)	Sensor/ channel name	Peak Sensitivity dB ref. 1 V/(m/s)
1	WDI	100–1000 (125)	CH2	96
2	R15I	50–200 (75)	CH5	109
3	R6I	40–100 (55)	CH6	117

greater than M^o, *'a'* and *'b'* are positive constants. For analysis of acoustic emission data the magnitude M is replaced by $A_{dB}/20$. Therefore, the GR relation can be written as $log_{10} N(A_{dB} \geq A_{dB}°) = a - b\frac{A_{dB}}{20}$ for AE data. This relation is successfully used for the scaling of amplitude distribution of AE waves and the previous research, particularly on concrete, show that the b-value changes systematically during the different stages of the failure process (Carpinteri et al., 2009). This approach is based on: (i) the analogy between the damage phenomenon within a material and seismic activity in given region of earth's crust; and (ii) scale independent character of b-value (Lockner, 1993; Carpinteri et al., 2012). The b-value is generally estimated by least square (LS) and maximum likelihood method (MLM). The literature suggests that the b-values estimated using maximum likelihood method are more reliable in comparison to the least square estimated values as the latter may be biased and influenced by large events (Amitrano, 2012, Amorese et al., 2009). Therefore, in the present analysis b-value was estimated by the method of maximum likelihood following AKI (1965) formulation:

$$b = \frac{20 * log_{10}(e)}{(< A_{dB} > - A_{dB}°)} \quad (2)$$

where $< A_{dB} >$ is arithmetic mean of 40 amplitude values of a particular window and A_{dB}^o is the minimum amplitude (or threshold limit) of the same window. The time shown for each estimated b-value was the time of the 40th amplitude value of the corresponding window. This process was repeated for all the amplitude values of AE events from beginning to the end of each experiment.

AE data was further used for the classification of cracking/fracture mode based on two parameters namely, RA value and average frequency (AF) (JCMS-III, 2003, Li and Du, 2016). Parameter RA is defined as the ratio of rise time to amplitude, while AF is calculated by dividing counts with the duration of acoustic wave. In the present study, ice samples were deformed under the action of external force applied through constant displacement rate. If there is no heat exchange between specimen and surroundings, the total work done by external force on the specimen can be considered as total strain energy input (Liu and Liu, 2016; Zhang et al., 2014) as shown below:

$$U^t = U^e + U^d \quad (3)$$

where U^t is the total elastic energy input, U^e is the recoverable elastic energy; U^d is the dissipated energy. In fact the energy released during damage/crack initiation within material is not fully dissipated and a portion of this energy further excites transient dynamic motion in the form of AE (Carpinteri et al., 2016; Doll, 1984; Sharon et al., 1996). Further Doll (1984) and Gross et al., 1993 suggest that only 3% of the total fracture energy could be associated with AE and most of the stored energy is dissipated as heat. Schematic diagram to depict the relation between the elastic energy and dissipated energy is shown in Fig. 2. The total input strain energy imparted to the specimen during the process of loading was calculated from the area under the experimental stress-strain curve using Eq. 4. Recoverable elastic energy was calculated from the experimental stress values and modulus of elasticity of ice as given in Eq. 5.

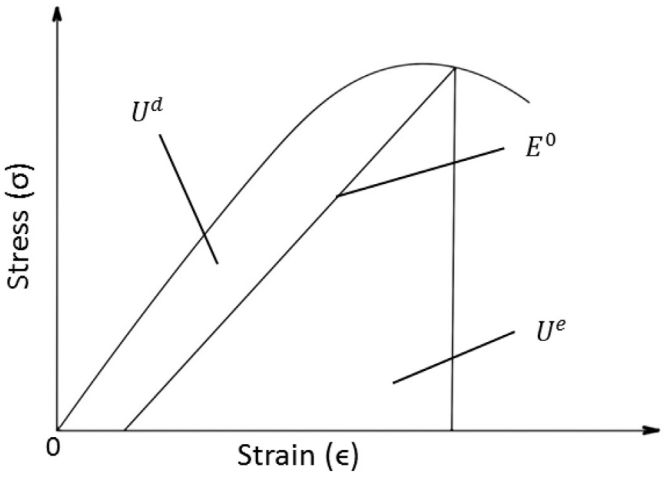

Fig. 2. Schematic to represent the components of total mechanical energy.

$$U_{cum}^{t} = \sum_{i=2}^{n-1} \sigma_i \varepsilon_i - \frac{(\sigma_1 + \sigma_n)}{2} \Delta\epsilon \quad (4)$$

$$U_{cum}^{e} = \sum_{i=1}^{n} \frac{\sigma_i^2}{2E} \quad (5)$$

The symbols represent: σ is bending stress, ϵ is strain, E is modulus of elasticity, $U_{cum}{}^{t}$ is cumulative input strain energy, and $U_{cum}{}^{e}$ is cumulative elastic energy.

The dissipated energy during the plastic deformation or micro-cracking in ice sample was computed by subtracting elastic energy from total input energy as per Eq. 3.

In the present paper, acoustic energy release rate and cumulative acoustic energy was calculated and compared with dissipated energy for all the three tests. Acoustic emission (AE) energy mentioned in the paper is 'absolute acoustic energy' which is defined as the measured area under the rectified signal envelope (MARSE) of AE wave (Miller et al., 2005). The dissipated mechanical energy is commonly recognized as a good indicator of damage in the structure (Sagasta et al., 2016; Vidya Sagar and Raghu Prasad, 2012).

3. Results and discussion

3.1. AE signatures analysis

3.1.1. AE parameters: hits and amplitude analysis

Fig. 3 (a) in each panel (i.e Panel 1, 2 and 3) shows the stress and strain behaviour corresponding to three strain rates i.e. 1×10^{-5} s^{-1} (SR1), 1×10^{-4} s^{-1} (SR2) and 1×10^{-3} s^{-1} (SR3), respectively. The analysed data during the present experiment was recorded using three AE sensors, namely CH2, CH5 and CH6 coupled directly on the surface of the ice specimen. The average flexural strength of ice specimen was 0.86 MPa. Fig. 3(b) and Fig. 3(c) in each panel show temporal distribution of AE amplitude and cumulative AE hits, respectively. Each data point in the scatter of amplitude distribution plot represents an AE hit which is analogues to a plastic deformation/failure event occurring within the material. These microscopic fractures may arise due to movement of dislocations, opening of crack etc. within the ice specimen. Largest voltage present in a hit (i.e. AE signal) is referred to as AE amplitude. A distinct difference in the amplitude values of AE can be seen in the Fig. 3(b) of each panel. In SR1 the low level of AEs mostly below the 40 dB amplitude were emitted till the failure of ice specimen. Only 20% of the AEs having amplitude more than 40 dB were recorded for SR1 as compared to the ~40% in case of SR2 and SR3 prior to ultimate failure. The average amplitude was found 36 dB for SR1 and ~ 42 dB for both SR2 and SR3. During initial loading stage the ice beam stabilizes itself on two simply supported cylinders over its span. In case of SR1 and SR2, the AE generated during initial stage was followed by a silent period till the applied stress reaches 11% and 5% of ultimate stress, respectively. However in SR3 the loading rate is very high which causes the damage and crack propagation in specimen from the very beginning and large AE activity is recorded. Li and Du, 2016, have also reported similar behaviour during the compression and flexural test of ice samples. They have attributed that the AE emitted for stress values less than 30% of failure stress is mostly due to the friction and external noise. Scatter plot in Fig. 3(b) of Panel1 further reveals that the AE in case of lowest strain rate i.e. SR1 (1×10^{-5} s^{-1}) are of very low amplitude throughout the loading process except at failure of specimen. According to Weiss et al. (2000), there are two different mechanisms mainly responsible for acoustic emission activity in ice: high velocity motion of dislocations and

crack nucleation and propagation. Dislocations, the linear defects within a crystal structure, are produced during crystallization or diffusion process. They can also be generated during the plastic deformation of ice which is governed by the dislocation dynamics under the influence of applied stress (Petrenko and Whitworth, 2006; Montagnat and Duval, 2004). Weiss et al. (2000) have experimentally shown that AEs of significant amplitude were emitted from polycrystalline ice during compression without the onset of micro-cracking. Therefore the main source of emitted AE was attributed to dislocation dynamics. In the case of SR1 no visual cracks were seen for a long time, even though the low level of AEs were continuously emitted. Sinha, 1985, also reported very low amplitude AEs before the onset of visible micro-cracking in sea ice during uniaxial compression. Fig. 3(b) of both Panel 2 & 3 depict that very high amplitude AEs are accompanied with low level emissions because both mechanisms (i.e. dislocation movement and crack opening) may be contributing for AE generation dominated by the opening of cracks. It is interesting to note that, very high amplitude AE burst emissions were associated with the ultimate failure of ice specimen in all the three cases. Langhorne and Haskell (1996) have also reported largest value of AE energy released during the fracture of cantilever beam of sea ice.

The temporal variation of cumulative hits shows the emission rate and total activity detected during the complete tests is shown in Fig. 3 (c) of each Panel. The gradient of cumulative AE shows an increasing trend from low strain rate SR1 to the high strain rate SR3. Average AE hit rate was calculated by dividing the total number of hits recorded in particular test with the respective experiment duration. The variation of AE hit rate with strain rate is shown in semi-log plot (Fig. 4). The hit rate increased from SR1 to SR3 following a power law with an exponent of 1.09 ($R^2 = 0.98$).

AE counts and wave duration were also analysed with respect to amplitude distribution. For strain rate SR2, Fig. 5(a) and 5(b) show the temporal variation of AE amplitude and counts and cross-plot between them respectively. AE count represents the number of times AE wave crossed the threshold amplitude level during a particular hit. It can be seen that numbers of counts vary in a large range from very low i.e. 1 to more than 10,000 near the catastrophic failure. Overall there was a variation of four orders of magnitude in the number of counts. The increase in amplitude is associated with a substantial increase in the AE count number. Further from Fig. 5(b), it can be observed that AE counts are more than 500 corresponding to the amplitude values more than 60 dB. The average count rates (counts/s) were found to be 185, 3714 and 42,075 for strain rates SR1, SR2 and SR3, respectively. More or less similar behaviour was shown by all the three tests (i.e. SR1, SR2 & SR3) and for all the AE sensors.

Temporal variation of AE wave duration with AE amplitude is shown in Fig. 6. Here also the wave duration increases with increase in the AE amplitude. It can be inferred that the micro-failure event having large AE amplitudes are associated generally with long AE waveforms. Majority of AE hits were having the wave duration between 10 μs to 10^4 μs. Very long AE waves were observed near the failure of the ice sample. This may be due to the large chain of events occurring near failure and superimposing on each other resulting in a single AE hit of long duration. Very long duration of AE waves were also reported by Li and Du (2016) in their experiments on ice specimen close to the critical failure. However, Sinha (1994) found varying AE wave durations corresponding to the sea ice and shelf ice. Sea ice was having a lesser magnitude of about two orders as compared to shelf ice which was having four orders of magnitude. Further, the large AE wave duration was attributed to the large size of cracks.

3.2. b-value analysis from AE amplitude data

Fig. 7 shows the variation of AE cumulative frequency of occurrence vs peak amplitude plots corresponding to three different strain rates. It can be observed that AE events with large amplitudes are relatively less in number as compared to the smaller AE amplitudes. This phenomenon is analogous to the magnitude variation in earthquakes, concrete, rock failure [Colombo et al., 2003; Vidya Sagar et al., 2012, Cox and Meridith, 1993; Rao and Lakshmi, 2005)].

Temporal variation of b-value for all the three strain rates is shown

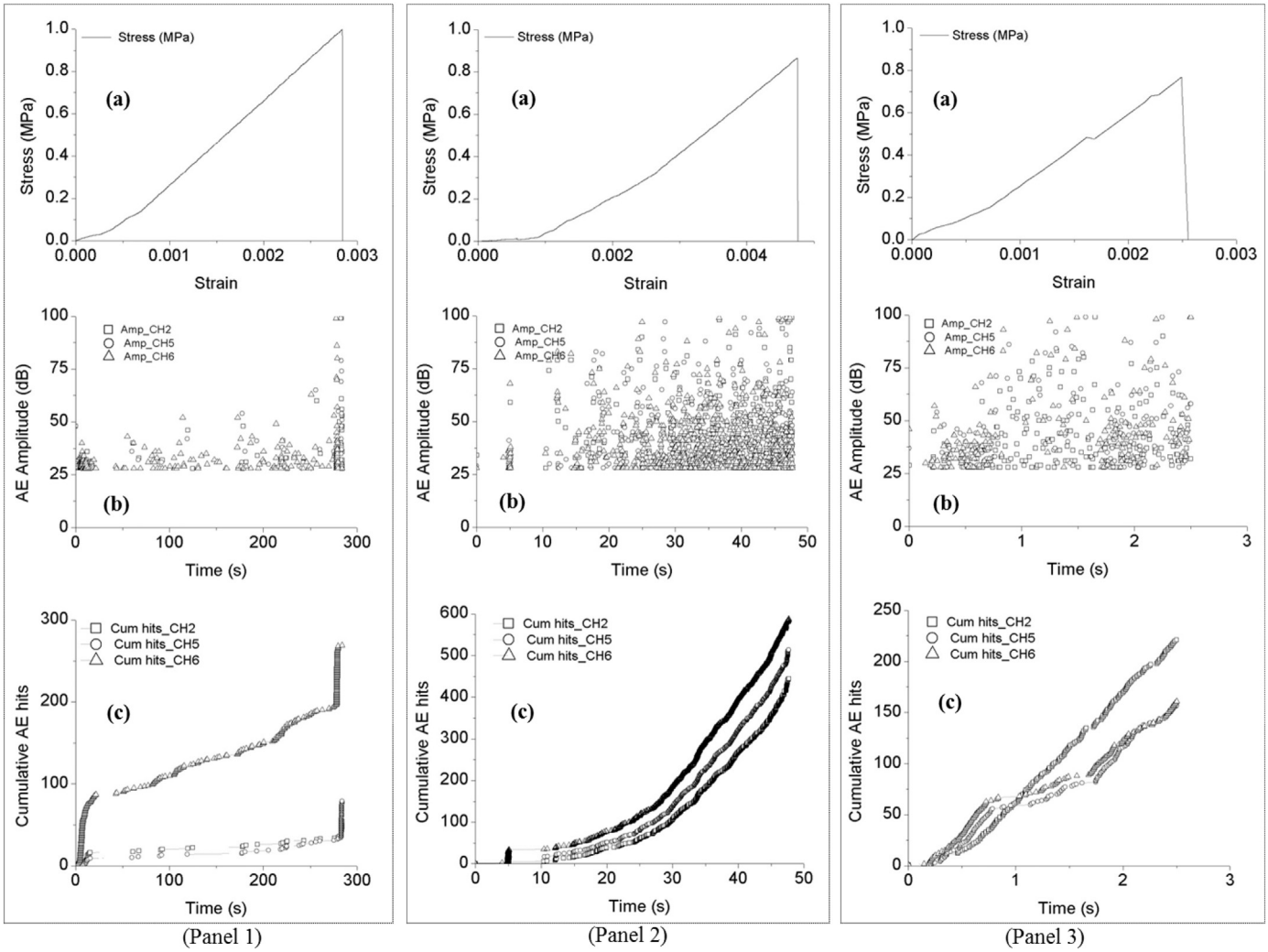

Fig. 3. Panel (1) represent: (a) Stress-strain behaviour of ice specimen, (b) AE amplitude distribution, (c) Cumulative AE hits, corresponding to strain rate $1 \times 10^{-5}\ s^{-1}$(SR1); Panel (2) represent: (a) Stress-strain behaviour of ice specimen, (b) AE amplitude distribution, (c) Cumulative AE hits, corresponding to strain rate $1 \times 10^{-4}\ s^{-1}$ (SR2); Panel (3) represent: (a) Stress-strain behaviour of ice specimen, (b) AE amplitude distribution, (c) Cumulative AE hits, corresponding to strain rate $1 \times 10^{-3}\ s^{-1}$(SR3).

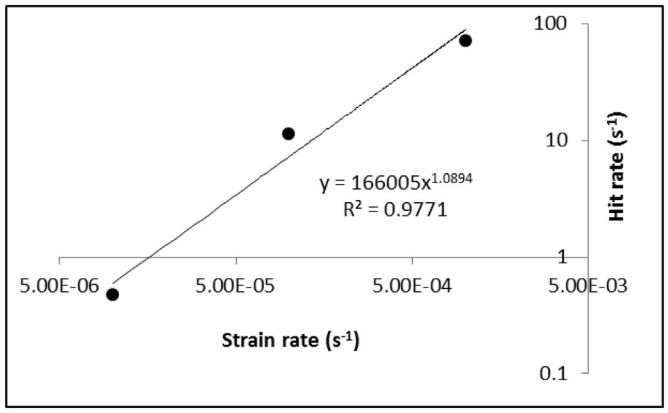

Fig. 4. AE hits rate (average of all 03 channels used in analysis) corresponding with strain rate.

in Fig. 8. It can be seen that b-value shows a global decreasing trend with increase in load for all the strain rates. In case of SR1 i.e. $1 \times 10^{-5}\ s^{-1}$, very high initial b-value was observed mainly because of the emissions of very low amplitude AEs [(Fig. 3(b), Panel 1]. Thereafter, the b-value decreased gradually till the load was 74% of peak load and a sharp decrease was observed just before the failure of the specimen. However, in case of SR2 and SR3 the initial b-value is ~1 and decreases to ~0.4 at the sample failure. The b-value curve is relatively smooth for SR1 and SR3, however, in case of SR2 many fluctuations were observed. Because of limited data points in case of SR1 and SR3 the inherent fluctuations in b-value might not have been captured during its temporal evolution. From the load-time curve of SR1 and SR2, it can be seen that failure of ice specimen occurs suddenly without any distinct visible damage accumulation in terms of mechanical response. However, the emitted AEs and b-value trend suggest existence of the damage process during loading of ice specimen. Similar behaviour has also been reported by Schiavi et al. (2011) for concrete specimen during compression test. The b-value suddenly drops for SR3 just before a visible drop in load-time curve; thereafter the b-value remains almost same till final failure of specimen. The overall variations in b-value for all three cases suggest the existence and evolution of different degree of damage at different strain rates. Previous researchers suggest that at the condition of criticality, the temporal evolution of b-value is mainly governed by two mechanisms, i.e. fracture nucleation and fracture growth (Carpinteri et al., 2009). They further suggest that in the initial part of loading process micro-fractures are always evenly distributed around the initial notch termed as

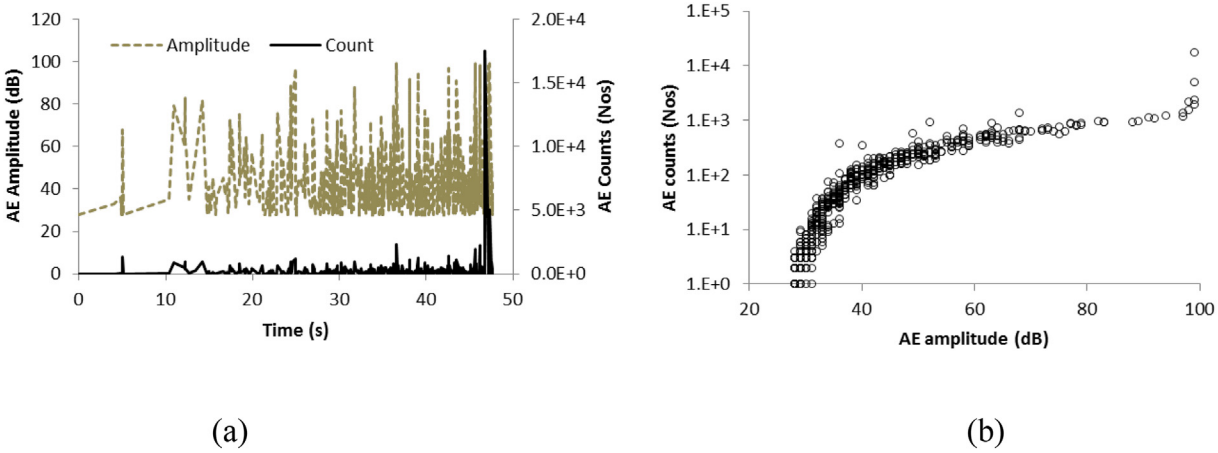

Fig. 5. (a) Temporal variation of AE amplitude (dB) and AE counts (in numbers.); (b) Cross plot between AE counts and AE amplitude; *(The data of strain rate SR2, CH no 06)*.

'fracture process zone'. However, at the final collapse the damaging process localizes near final failure surface through the rapid crack growth and coalescence within structure which is further attributed to the drop in b-value (Vidya Sagar et al., 2012). In the present analysis, the temporal evolution of b-value for strain rate SR1 may be largely dominated by the nucleation and growth of micro-cracks within ice specimen around the failure surface till it reaches to the final collapse. On the other hand, for higher strain rates i.e. SR2 and SR3, all the three mechanism i.e. formation, growth and coalescence of micro-crack may be active from the beginning of the loading test. This can be further supported by the AE amplitude distribution data [Fig. 2(b), Panels 2 & 3] which shows that very high amplitude AEs emit just after the loading process is started. Li and Du (2016) also observed the drop in b-value from 1.1 at the initial loading to the 0.5 at the final collapse of ice specimen. The variation in b-value was attributed to the damage caused by the development, expansion and interconnection of cracks in specimen under three point beam test. Thus monitoring of b-value variation can be an effective tool to assess the failure process in ice structure under stress.

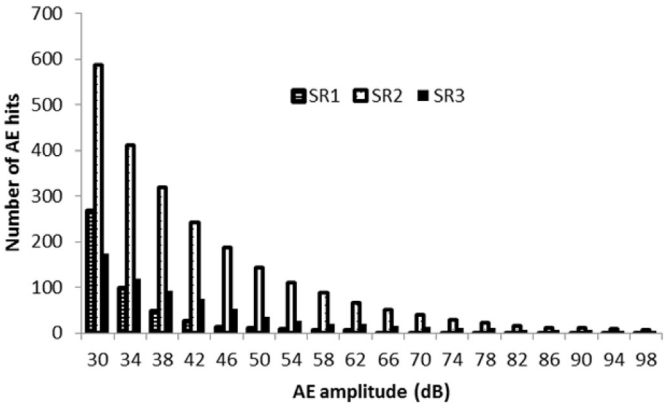

Fig. 7. Variation of AE hits with amplitude corresponding to strain rates: SR1 (1×10^{-5} s^{-1}), SR2 (1×10^{-4} s^{-1}) and SR3 (1×10^{-3} s^{-1}).

3.2.1. AE energy

Fig. 9 (a,b,c) shows the variation of AE energy and cumulative AE energy with time for all three strain rates, SR1, SR2 and SR3, respectively. The AE energy emission behaviour is strongly dependent on the strain rate. A large difference in AE energy exists corresponding to the three strain rates. The cumulative energy for SR1 is below ~10^4 aJ and increases abruptly at the time of ultimate failure of the ice sample. However, in case of SR2 and SR3 the cumulative energy is comparatively higher of the ~10^6–10^8 aJ. Also, it can be seen that total cumulative energy is of the same order at failure of ice sample irrespective of the strain rates. Low AE energy for SR1 for a long time may be attributed to the low level of damage within the ice specimen. Multiple high energy spikes observed in plots 9(b) and 9(c) are associated with the micro-fractures undergoing in ice specimen at higher strain rates.

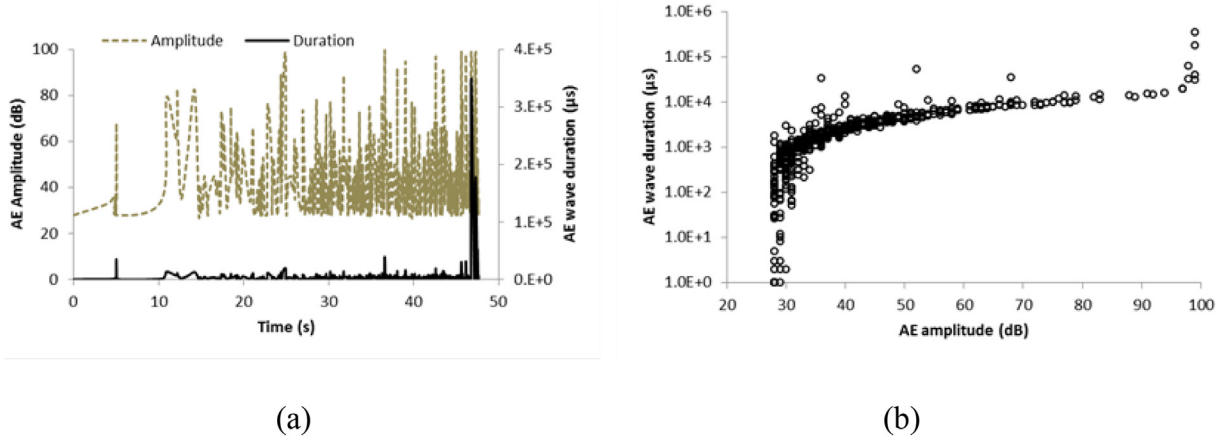

Fig. 6. (a) Temporal variation of AE amplitude (dB) and wave duration (µs); (b) Distribution of AE wave duration with AE amplitude; *(The data of strain rate SR2, CH no 06)*.

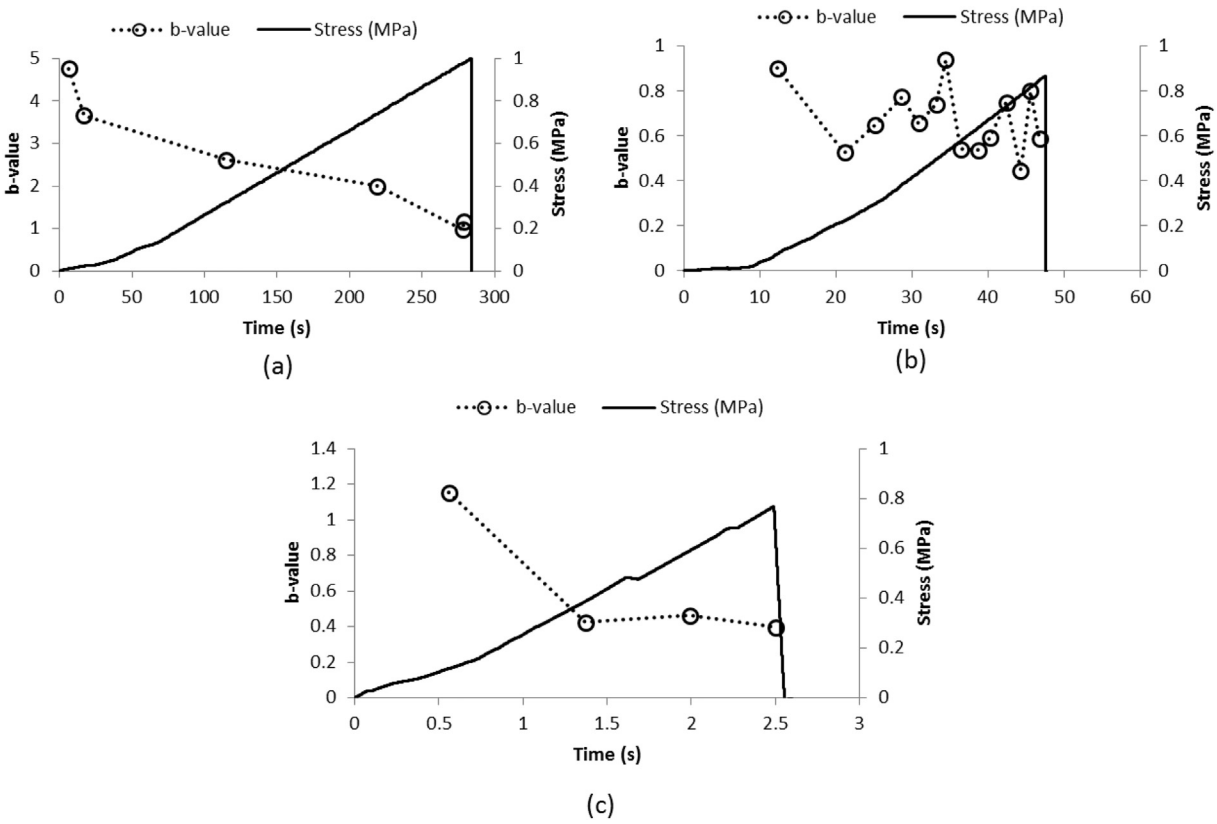

Fig. 8. Temporal variation of b-value with loading process corresponding to strain rates: (a) SR1 ($1 \times 10^{-5}\ s^{-1}$), (b) SR2 ($1 \times 10^{-4}\ s^{-1}$) and (c) SR3 ($10^{-3}\ s^{-1}$).

A comparison of cumulative dissipative energy and acoustic energy is shown in Fig. 10. The variation of both the energies follow more or less similar trend with sudden increase at the fracture of ice specimen. Though, one to one comparison of absolute values of both the energies is not possible because of: (i) very inefficient conversion mechanism of released fracture energy to elastic stress waves, (ii) filtering of very low amplitude emissions due to amplitude threshold setting while acquiring the AE data, (iii) propagation losses in AE signal within material and at

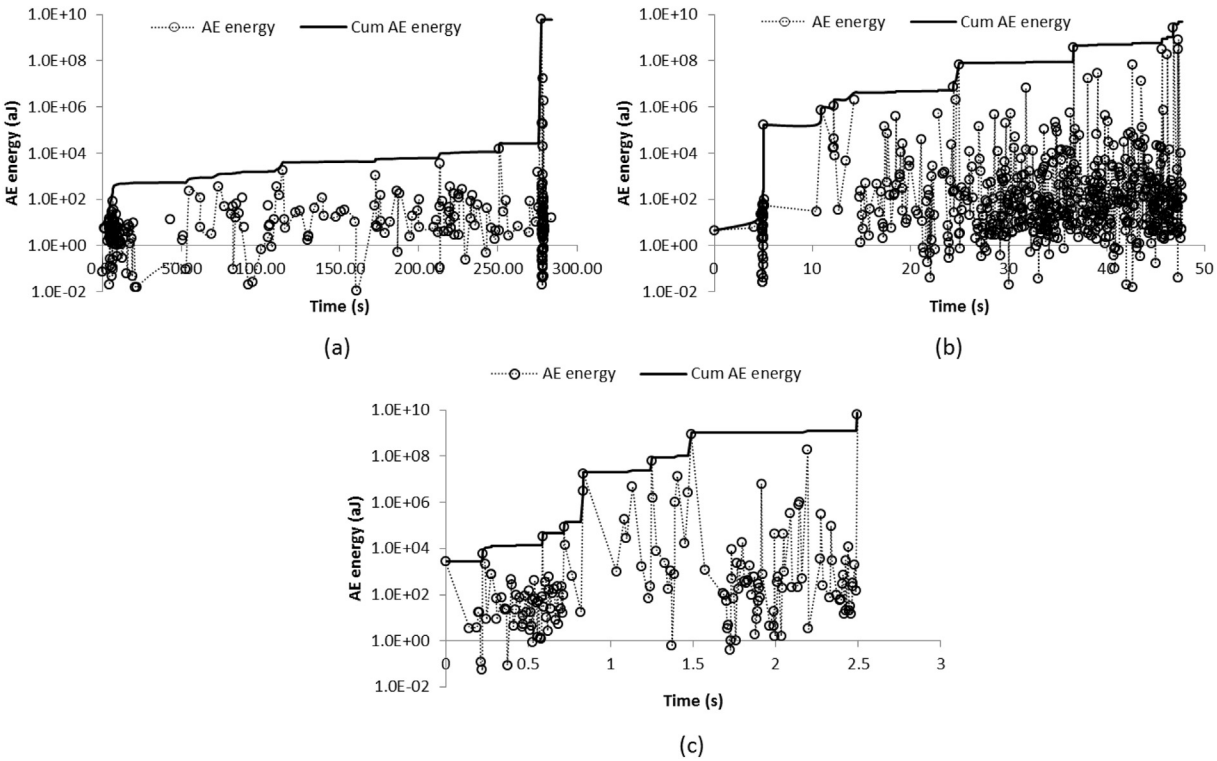

Fig. 9. Temporal variation of AE energy and cumulative AE energy: (a) SR1 (1×10^{-5}) s^{-1}; (b) SR2 (1×10^{-4}) s^{-1}, and (c) SR3 (1×10^{-3}) s^{-1}.

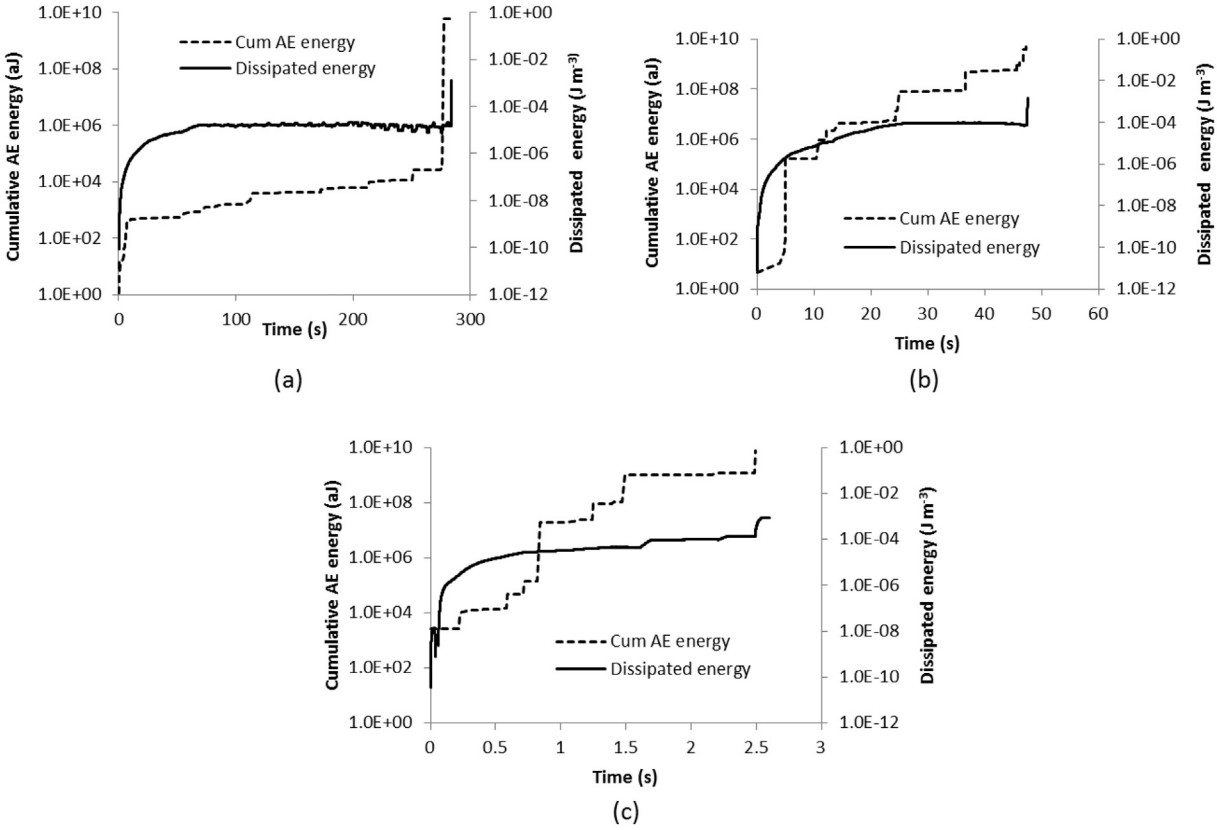

Fig. 10. Comparison of cumulative AE energy and dissipated mechanical energy for strain rates: (a) SR1 ($1 \times 10^{-5}\ s^{-1}$), (b) SR2 ($1 \times 10^{-4}\ s^{-1}$), and (c) SR3 ($1 \times 10^{-3}\ s^{-1}$).

boundaries. Sagasta et al., 2016 also found good agreement between plastic strain energy and acoustic emission energy during the experimental investigation on reinforced concrete structures. Researchers have carried out investigations to study the relationship between fracture energy of concrete and AE energy released (Landis and Baillon, 2002; Vidya Sagar and Raghu Prasad, 2008). They reported a clear correlation, with a large scatter, between fracture energy and acoustic emission energy. However, Carpinteri et al. (2016) found that the fracture energy increases with the specimen size whereas the AE energy decreases. They concluded that direct relationship cannot be established between the two forms of energies. Therefore, further experimental and theoretical investigations in this direction are required to establish the relationship (if any) between the two energies.

3.2.2. Identification of fracture modes

AE waveforms generated from a material under stress carry the information about its damage mechanism at different scales. Identification of fracturing mode can be done by analysing the parameters rise angle (RA) and average frequency (AF) (Ohno and Ohtsu, 2010; Aggelis, 2011; Lacidogna et al., 2017; Li and Du, 2016). AE waveform characteristics such as rise time, amplitude, counts and duration are used to derive the RA and AF values. Fig. 11 shows the variation of AF and RA with three strain rates SR1, SR2 and SR3. Each plot shows the relationship between AF and RA values estimated corresponding to each AE sensor used in the study. It can be observed that the RA values are mostly below 50 μs/dB for all the three strain rates SR1, SR2 and SR3.

Very few events have achieved RA values beyond 50 μs/dB. However, in case of strain rate SR3 many scattered AE events have shown the RA beyond 50 μs/dB. The average frequency varied mostly up to 200 kHz in all the cases. Few AE events in each case have AF values up to 300 KHz. The small RA represents the sudden fracture in the specimen. Majority of AE events with smaller RA value suggest the dominance of tensile mode (Mode I) of fracture in the ice specimen throughout the experimental period (Ohno and Ohtsu, 2010; Vidya Sagar, 2017). These results are in agreement to the earlier work of Li and Du, 2016. Their findings suggest that development of tensile cracks mainly control the failure process of ice specimen during three point bending. The scatter in the RA values may be attributed to the mix-mode failure of ice sample due to heterogeneity at the microstructure level. In fact the propagation of crack within ice sample is always tortuous which is responsible for asymmetric loading axis and hence leads to development of both tensile as well as small amount of shear loading also.

4. Conclusions

Acoustic emission is evolving as a potential technique for monitoring deformational processes in various materials. It is a passive method and listens the sound of cracks in high frequency range. In the present study we have employed AE to study the deformation/failure of ice specimen subjected to three points bending at different strain rates. AE was measured simultaneously by coupling the sensors directly on the surface of ice specimen in a cold room at −9 °C. The average flexural strength of ice specimen was 0.86 MPa. Various AE characteristics such as amplitude, energy, counts, wave duration were analysed. Amplitude distribution data was used to derive temporal evolution of b-value along with load. In all the three strain rates the b-value was found decreasing and attains minimum value near failure of the ice beam. For the identification of fracture mode, parameters such as RA and AF were analysed. It was observed that the failure of ice beam was dominated by the tensile crack during three point bending.

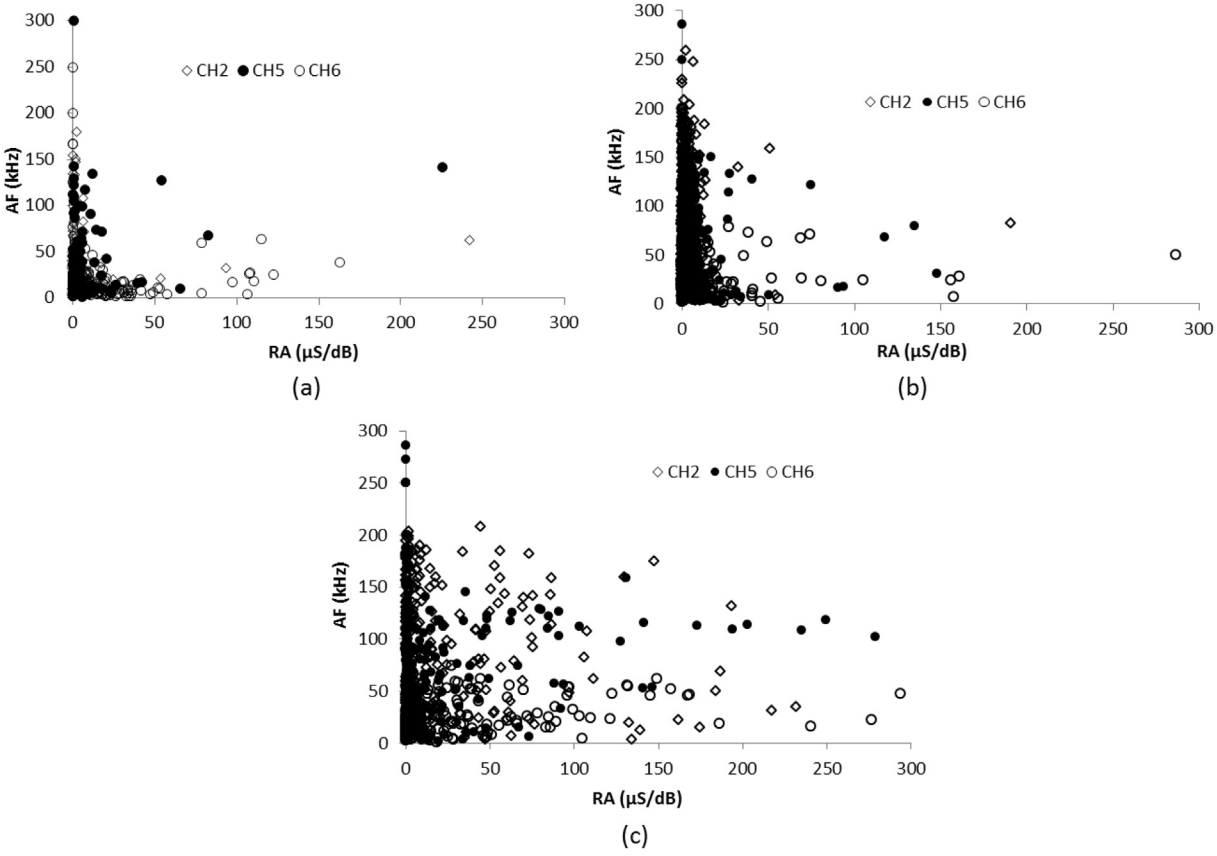

Fig. 11. RA parameter and average frequency (AF) correlation; (a) for strain rates SR1 ($1 \times 10^{-5}\ s^{-1}$), (b) SR2 ($1 \times 10^{-4}\ s^{-1}$) and (c) SR3 ($1 \times 10^{-3}\ s^{-1}$).

Authors contributions

P.D. conceptualized, analysed the presented data and was the major contributor in writing this paper. C·C contributed in experimentation, formulation and analysis, V.K. was mainly responsible for sample preparation, conduction of experiment and data analysis, R.S. assisted in data analysis. D. N. Assisted in AE data collection, J.C.K. & P.K.S. reviewed the analysis of the data and contributed to the interpretation of the results.

Declaration of Competing Interest

The authors declare that they have no known competing financial interests or personal relationships that could have appeared to influence the work reported in this paper.

Acknowledgements

The authors express their gratitude to Naresh Kumar, Director, SASE for his constant encouragement to carry out this work. We wish to thank P. K. Satyawali for discussions on various issues related to the AE based experimental investigation. The authors gratefully acknowledge the help extended by Karamjeet Singh, Rajiv Kumar, Manoj Kumar, Mehraj Middya during sample preparation and execution of experimental work in Cold Lab Manali. We are grateful to the anonymous reviewers for their comments that helped to improve the quality and presentation of the paper.

Appendix A. Calculation of the flexural stress for a rectangular cross section (b x d) and span length L

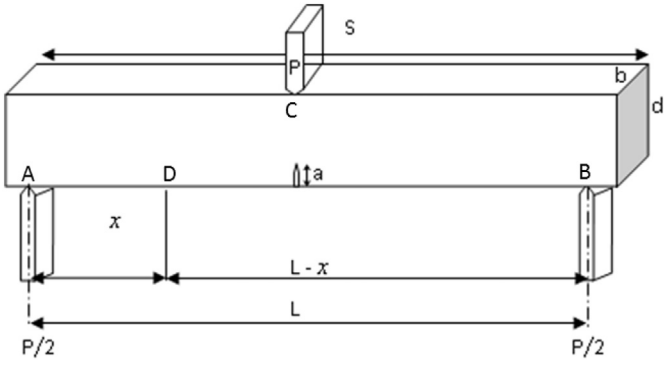

Fig. A1. Schematic diagram of test setup.

As shown in Fig. 1 the beam is simply supported at points A and B and displacement rate was applied at centre point C. Bending moment, M at any point D at a distance x from point A:

$$M_x = P\,x/2 \tag{1}$$

where P is the load, recorded at centre through load cell in response to deformation rate.

For rectangular cross-section Moment of inertia, $I = bd^3/12$ and Section Modulus, $Z = bd^2/6$.

According to the beam theory:

$$\frac{M}{I} = \frac{\sigma_f}{y} = \frac{E}{R} \tag{2}$$

where σ_f is failure stress, E is modulus of elasticity and R is radius of curvature

$$\sigma_f = \frac{M}{I}y = \frac{M}{Z} = \frac{3PL}{2bd^2} \tag{3}$$

For Strain.

$$\text{as } \frac{M}{I} = \frac{\sigma_f}{y} = \frac{E}{R} \therefore \frac{1}{R} = \frac{\partial^2 y}{\partial x^2} = \frac{P\,x}{2EI} \tag{4}$$

Solving Eq. (4) deflection at any point D is

$$\Delta = \frac{P\,x^3}{12EI} - \frac{PL^2}{16EI}\,x \tag{5}$$

Deflection at x = L/2: $\Delta_{max} = \frac{PL^3}{96EI} - \frac{PL^3}{32EI} = -\frac{PL^3}{48EI}$ or $-\frac{ML^2}{12EI}$.

Therefore modulus of elasticity E_f,

$$E_f = \frac{PL^3}{48\Delta_{max} I} = \frac{PL^3}{48\Delta_{max}\left(\frac{bd^3}{12}\right)} = \frac{PL^3}{4bd^3\Delta_{max}} \tag{6}$$

as $\sigma_f = \epsilon_f E_f \therefore \epsilon_f = \frac{\sigma_f}{E_f}$ using Eq. (3) and Eq. (6)

$$\epsilon_f = \frac{\left(\frac{3PL}{2bd^2}\right)}{\left(\frac{PL^3}{4bd^3\Delta_{max}}\right)} = \frac{6d}{L^2}\Delta_{max} \tag{7}$$

Differentiating both side gives

$$\dot{\epsilon}_f = \frac{6d}{L^2}\dot{\Delta}_{max} \tag{8}$$

Eq. (8) is used to determine the displacement rate ($\dot{\Delta}_{max}$) corresponding to the strain rate at which ice samples were tested.

References

Aggelis, D.G., 2011. Classification of cracking mode in concrete by acoustic emission parameters. Mech. Res. Commun. 38 (3), 153–157.

AKI, K., 1965. Maximum likelihood estimate of b in the formula log (N) =a− bM and its confidence limits. Bull. Earthq. Res. Inst. 43, 237–239 Tokyo Univ.

Amitrano, D., 2012. Variability in the power-law distributions of rupture events. Eur. Phys. J. Spec. Topics 205 (1), 199–215.

Amitrano, D., Grasso, J., Senfaute, G., 2005. Seismic precursory patterns before a cliff collapse and critical point phenomenon. Geophys. Res. Lett. 32 (L08314).

Amorese, D., Grasso, J.R., Rydelek, P.A., 2009. On varying v-valueswith depth: results from computer-intensive tests for Southern California. Geophys. J. Int. 1–14.

Andrews, R.M., 1985. Measurement of the fracture toughness of glacier ice. J. Glaciol. 31 (108), 171–176.

Bucur, V., 2006. Acoustics of Wood, 2nd ed. Springer, Berlin.

Carpinteri, A., Lacidogna, G., Puzzi, S., 2009. From criticality to final collapse: evolution of the “b-value” from 1.5 to 1.0. Chaos. Solitons Fractals 41, 843–853.

Carpinteri, A., Corrado, M., Lacidogna, G., Puzzi, S., 2012. Three different approaches for damage domain characterization in disordered materials: Fractal energy density, b-value statistics, renormalization group theory. Mech. Mater. 53, 15–28.

Carpinteri, A., Lacidogna, G., Accornero, F., Mpalaskas, A.C., Matikas, T.E., Aggelis, D.G., 2013. Influence of damage in the acoustic emission parameters. Cem. Concr. Compos. 44, 9–16.

Carpinteri, A., Lacidogna, G., Corrado, M., Battista, S., 2016. Cracking and crackling in concrete-like materials: a dynamic energy balance. Eng. Fract. Mech. 155, 130–144.

Chandel, C., Srivastava, P.K., Mahajan, P., 2014. Determination of failure envelope for faceted snow through numerical simulations. Cold Reg. Sci. Technol. 101, 14–23.

Colombo, I.S., Main, I.G., Forde, M.C., 2003. Assessing damage of reinforced concrete beam using b-value analysis of acoustic emission signals. J. Mater. Civ. Eng. ASCE 280–286.

Cox, S.J.D., Meridith, P.G., 1993. Microcracking formation and material softening in rock measured by monitoring acoustic emissions. Int. J. Rock Mech. Min. Sci. Geomech. Abstr. 30 (1993), 11–24.

Datt, P., Kapil, J.C., Kumar, A., 2015. Acoustic emission characteristics and b-value estimate in relation to waveform analysis for damage response of snow. Cold Reg. Sci. Technol. 119, 1–13.

Doll, W., 1984. Kinetics of crack tip craze zone before and during fracture. Polym. Eng. Sci. 24, 798–808.

Gold, L.W., 1960. The cracking activity in ice during creep. Can. J. Phys. 38 (9), 1137–1148.

Gross, S.P., Fineberg, J., Marder, M., McCormick, W.D., Swinney, H.L., 1993. Acoustic emissions from rapidly moving cracks. Phys. Rev. Lett. 71, 3162–3165.

Guarino, A., Garcimartin, A., Ciliberto, S., 1998. An experimental test of the critical behaviour of fracture precursor. Eur. Phys. J.B 6 (1), 13–24.

Gutenberg, B., Richter, C.F., 1944. Frequency of earthquakes in California. Bull. Seismol. Soc. Am. 34, 185–188.

Hellier, C.J., 2003. Handbook of Non-Destructive Evaluation, 2nd ed. The McGraw-Hill Companies, Inc., USA.

JCMS-III B5706, 2003. Monitoring Method for Active Cracks in Concrete by Acoustic Emission. Federation of Construction Materials Industries, Japan.

Kapil, J.C., Datt, P., Kumar, A., Singh, K., Kumar, V., Satyawali, P.K., 2014. Multi-sensor couplers and waveguides for efficient detection of acoustic emission behaviour of snow. Cold Reg. Sci. Technol. 101, 1–13.

Lacidogna, G., Piana, G., Carpinteri, A., 2017. Acoustic emission and modal frequency variation in concrete specimens under four-point bending. Appl. Sci. 7 (339), 2–14. https://doi.org/10.3390/app7040339.

Landis, E.N., Baillon, L., 2002. Experiments to relate acoustic emission energy to fracture energy of concrete. J. Eng. Mech. 128 (6), 698–702.

Langhorne, P.J., Haskell, T.G., 1996. Acoustic emission during fatigue experiments on first year sea ice. Cold Reg. Sci. Technol. 24, 237–250.

Li, D., Du, F., 2016. Monitoring and evaluating the failure behaviour of ice structure using the acoustic emission technique. Cold Reg. Sci. Technol. 129, 51–59.

Liu, X., Liu, J., 2016. Analysis on the mechanical characteristics and energy conversion of sandstone constituents under natural and saturated states. Adv. Mater. Sci. Eng. 2016, 1–14. https://doi.org/10.1155/2016/4360321. Article ID 4360321.

Lockner, D., 1993. The role of acoustic emission in the study of rock fracture. Int. J. Rock Mech. Min.Sci. Geomech. Abstr. 30 (7), 883–899.

Main, I.G., Meredith, G., Jones, C., 1989. A reinterpretation of the precursory seismic b-value anomaly from mechanics. Geophys. J. Int. 96, 131–138.
Masterson, D.M., 2009. State of the art of ice bearing capacity and ice construction. Cold Reg. Sci. Technol. 58 (3), 99–112.
Miller, R.K., Hill, E.K., Moore, P.O., 2005. Acoustic Emission Testing. NDT Handbook, 3rd ed. American Society for Nondestructive Testing, Columbus, OH, USA.
Montagnat, M., Duval, P., 2004. Dislocations in ice and deformation mechanism: from single crystal to polar ice. Defects Diffusion Forum 229, 43–54.
Ohno, K., Ohtsu, M., 2010. Crack classification in concrete based on acoustic emission. Constr. Build. Mater. 24, 2339–2346.
Ohtsu, M., 1996. The history and development of acoustic emissions in concrete engineering. Mag. Concr. Res. 48 (117), 321–330.
Petrenko, V.F., Whitworth, R.W., 2006. Physics of Ice. Oxford University Press, New York.
Pinzer, B.R., 2009. Dynamics of Temperature Gradient Snow Metamorphism: Microstructure Evolution and Transport Processes. Dissertation Doctor of Sciences ETH, Zurih.
Rao, M.V.M.S., Lakshmi, K.G. Prasanna, 2005. Analysis of b-value and improved b-value of acoustic emissions and accompanying rock fracture. Curr. Sci. 89, 1577–1582.
Reiweger, I., Mayer, K., Steiner, K., Dual, J., Schweizer, J., 2015. Measuring and localizing acoustic emission events in snow prior to fracture. Cold Reg. Sci. Technol. 110, 160–169.
Sagasta, F., Benavent Climent, A., Roldan, A., Gallego, A., 2016. Correlation of plastic strain energy and acoustic emission energy in reinforced concrete structures. Appl. Sci. 6 (84), 5–15. https://doi.org/10.3390/app6030084.
SAMOS AE system, User's Manual, 2005. Rev2. Physical Acoustics Corporation. Princeton Junction, NJ.
Schiavi, A., Niccolini, G., Tarizzo, P., Carpinteri, A., Lacidogna, G., Manuello, A., 2011. Acoustic emission at high and low frequencies during compression tests in brittle materials. Strain 47 (Suppl. 2), 105–110.
Shahidan, S., Pulin, R., Muhamad Bunnori, N., Holford, K.M., 2013. Damage classification in reinforced concrete beam by acoustic emission signal analysis. Constr. Build. Mater. 45, 78–86.
Sharon, E., Gross, S.P., Fineberg, J., 1996. Energy dissipation in dynamic fracture. Phys. Rev. Lett. 76, 2117–2120.
Shiotani, T., Aggelis, D.G., Makishima, O., 2007. Global monitoring of concrete bridge using acoustic emission. J. Acoust. Emission 25, 308–315.
Singh, K.K., Negi, H.S., Ganju, A., Kulkarni, A.V., Kumar, A., Mishra, V.D., Kumar, S., 2013. Crevasses detection in Himalayan glaciers using ground-penetrating radar. Curr. Sci. 105 (9), 1288–1295.
Sinha, N.K., 1985. Acoustic emission study on multi-year sea ice in an Arctic field laboratory. J. Acoust. Emission 4 (2/3), 290–293.
Sinha, N.K., 1994. Characteristics of acoustic emissions from different type of polycrystalline ice. In: Proc. International Symposium on Snow and Related Manifestations, 26–28 Sep 1994, Manali, India, pp. 176–183.
Sinha, N.K., 1996. Characteristics of acoustic emissions from different types of polycrystalline ice. In: Proceedings of the International Symposium on Snow and related Manifestations, Manali, India, 26-28 Sep 1994, pp. 176–183.
Sinha, N.K., Shkhinek, K., Smirnov, V., 2012. On borehole indenter (BHI) measurements and analysis. Cold Reg. Sci. Technol. 76-77, 109–120.
St Lawerence, W.F., Cole, D.M., 1982. Acoustic emissions from polycrystalline ice. Cold Reg. Sci. Technol. 183–199.
Vidya Sagar, R., 2017. Acoustic emission characteristics of reinforced concrete beams with varying percentage of tension steel reinforcement under flexural loading. Case Stud. Construct. Mater. 6, 162–176.
Vidya Sagar, R., Raghu Prasad, B.K., 2008. Relationship between AE energy and fracture energy of plain concrete beams: Experimental study. J. Mater. Civ. Eng. 20, 212–220.
Vidya Sagar, R., Raghu Prasad, B.K., 2012. A review of recent development in parametric based acoustic emission techniques applied to concrete structures. Nondestr. Test. Eval. 27 (1), 47–68.
Vidya Sagar, R., Raghu Prasad, B.K., Shantha Kumar, S., 2012. An experimental study on cracking evolution in concrete and cement mortar by the b-value analysis of acoustic emission technique. Cem. Concr. Res. 42, 1094–1104.
Weiss, J., Lahaie, F., Grasso, J.R., 2000. Statistical analysis of dislocation dynamics during viscoplastic deformation from acoustic emission. J. Geophys. Res. 105, 433–442.
Wikipedia, 2016. Siachen Glacier avalanche. https://en.wikipedia.org/wiki/2016_siachen_glacier_avalanche.
Zaretsky, Y.K., Fish, A.M., Gavirilo, V.P., Gusev, A.V., 1976. Short term ice creep and microcrack formation kinetics. CRREL Draft Trnaslation 539, 196–202.
Zhang, L., Ren, M., Ma, S., Wang, Z., 2014. Energy dissipation mechanism and damage model of marble failure under two stress paths. Frattura ed Integrita Strutturale 8 (30), 515–525.